

1
2
3
4
5
6
7
8
9
10
11
12
13
14
15
16
17
18
19
20
21
22
23
24
25
26
27
28
29
30
31
32
33
34
35
36

Non-tidal ocean loading signals of the North and Baltic Sea from terrestrial gravimetry, GNSS, and high-resolution modeling

C. Voigt¹, R. Sulzbach^{1,2}, H. Dobsław¹, A. Weise³, L. Timmen³, Z. Deng¹, M. Reich¹, N. Stolarczuk¹, H. Peters⁴, M. Fietz⁴, M. Thomas^{1,2} and F. Flechtner^{1,5}

¹ Helmholtz Centre Potsdam – GFZ German Research Centre for Geosciences, Potsdam, Germany

² Institute of Meteorology, Freie Universität Berlin (FUB), Berlin, Germany

³ Institute of Geodesy, Leibniz Universität Hannover (LUH), Hannover, Germany

⁴ Biologische Anstalt Helgoland, Alfred-Wegener-Institute (AWI), Helmholtz Centre for Polar and Marine Research, Germany

⁵ Institute of Geodesy and Geoinformation Science, Technische Universität Berlin (TUB), Berlin, Germany

Corresponding author: Christian Voigt (christian.voigt@gfz-potsdam.de)

Key Points:

- High-resolution ocean model of the North and Baltic Sea provides improved non-tidal ocean loading signals
- Model evaluation by geodetic observations on the island of Heligoland shows correlation of 0.9 and signal reduction of 50 %
- Additional continental gravimetric stations benefit from high-resolution model for an improved signal separation

Abstract

Non-tidal ocean loading signals are known to be a significant source of geophysically induced noise in gravimetric and geodetic observations also far-away from the coast and especially during extreme events such as storm surges. Operational products suffer from a low temporal and spatial resolution and reveal only small amplitudes on continental stations. Dedicated high-resolution sea-level modelling of the North and Baltic Sea provides a largely improved prediction of non-tidal ocean loading signals. Superconducting gravimeter and GNSS observations on the small offshore island of Heligoland in the North Sea are used for a thorough evaluation of the model values revealing correlations of up to 0.9 and signal reductions of up to 50 % during a storm surge period of one month in Jan-Feb 2022. Additional continental superconducting gravimeter stations are used to assess the benefits from high-resolution modelling for an improved signal separation further away from the coast.

37 Plain Language Summary

38 Terrestrial gravimetry is a technique to monitor temporal variations of the gravity acceleration at
39 the Earth's surface that are induced by mass variations and deformations caused by a large
40 number of geophysical effects on very different temporal and spatial scales. Current applications
41 of high social relevance are the estimation of terrestrial water storage variations under climate
42 change conditions, e.g., groundwater depletion or polar and alpine ice mass loss, as well as
43 hazard and geothermal monitoring. Before analysing such signals of interest, it is essential to
44 separate all other signals included in the gravimetric observations usually on the basis of
45 adequate models. Amongst these disturbing signals, non-tidal ocean loading is one of the smaller
46 but still significant effects. Up to now, the available operational products only show a weak
47 correlation with gravimetric observations and their application does not lead to a reduction of the
48 observational signal variation. This situation largely improves with a high-resolution model for
49 gravity observations on the North Sea island of Heligoland. The model results are also applied to
50 gravity records that were observed further away from the coast to assess the benefits of the
51 model for an improved signal separation even at continental stations.

52

53 1 Introduction

54 Gravimetric observations at the Earth's surface are affected by mass variations and
55 deformations of the Earth's crust induced by a large number of geophysical effects. While solid
56 Earth tides and ocean tide loading (OTL) are usually estimated from local tidal analyses of the
57 gravimetric observations, the effects of atmospheric mass-redistributions and Earth rotation are
58 computed by various services. Non-tidal ocean loading (NTOL) signals, largely caused by wind-
59 driven surges, are distinct at the coast, but through their large-scale characteristics significantly
60 affect gravimetric and geodetic observations up to several 100 km away from the coast. Hence,
61 for the analysis of terrestrial water storage variations or hazard and geothermal monitoring on
62 local or regional scales, the NTOL signals should be reduced from the observations. At present,
63 two operational products based on global ocean models are available for terrestrial gravimetry
64 that are both limited in temporal and spatial resolution: The EOST loading service (Boy, 2024)
65 provides daily NTOL model predictions based on ECCO2 in 0.25° resolution, while the
66 MATLAB toolbox mGlobe (Mikolaj et al., 2016) allows for the computation of NTOL
67 predictions from ocean bottom pressure anomalies of the GRACE Atmosphere and Ocean De-
68 Aliasing Level-1B (AOD1B RL07 and predecessor products) in 3h sampling up to degree and
69 order (d/o) 180 (Shihora et al., 2022; Dobslaw et al., 2017).

70 The analysis of NTOL signals with gravimetric observations has two limitations: First,
71 superconducting gravimeters are usually installed far away from the coasts in order to keep the
72 disturbing signals from the oceans small. Second, NTOL signals are often superimposed by
73 significant terrestrial water storage variations, since wind surges are often accompanied by heavy
74 precipitation events. To tackle these challenges, the small offshore island of Heligoland in the
75 North Sea (Figure 1) was chosen as study site (Voigt et al., 2023; Weise et al., 2020). It is
76 equipped with a redundant set of continuously operating sensors: two gravimeters, two GNSS
77 stations as well as two tide gauge stations.

78 Maximum NTOL signals of the North Sea were predicted by Fratepietro et al. (2006)
79 with gravity increases of 80 nm/s^2 and vertical displacements of 30 mm downwards during a

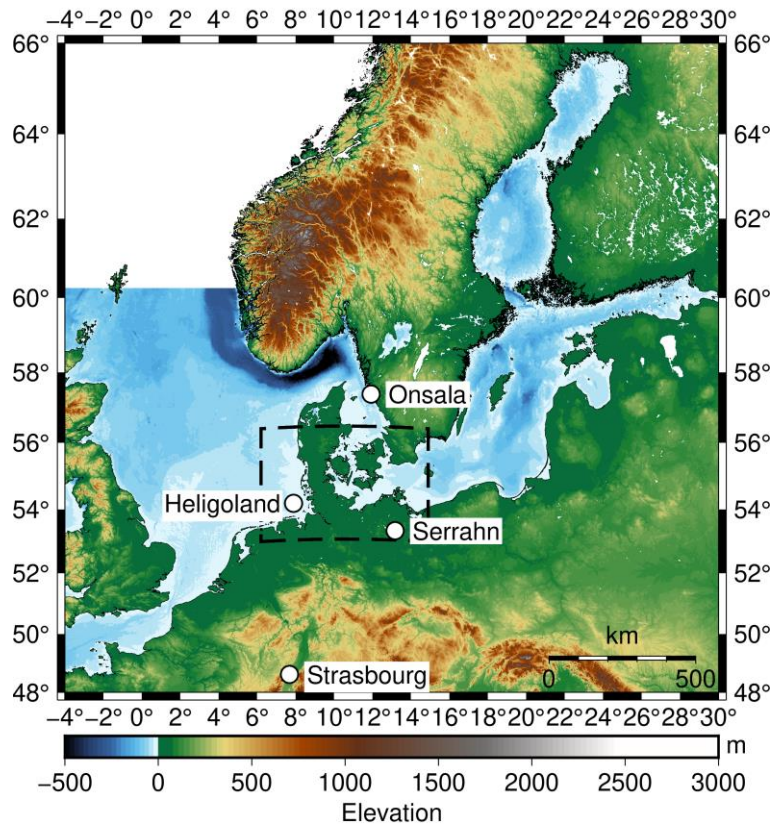


Figure 1. The Bathymetry of the North and Baltic Sea areas covered by the ocean model BSH-HBMnoku and adjacent topography with the four superconducting gravimeter stations under investigation. The dashed box indicates the fine resolution area of the model.

80 storm surge on 30 January 2000 with a local sea level of 2.7 m above mean high water (MHW)
 81 based on the Proudman Oceanographic Laboratory Storm Surge Model (POLSSM) with a
 82 resolution of approx. 12 km. The authors found some evidence of storm surge loading in the
 83 superconducting gravimeter (SG) data of Membach, which is 200 km away from the coast, and
 84 recommended a SG installation closer to the coast for NTOL signal enhancement. An extension
 85 of this study is provided by Boy and Lyard (2008), who applied 3D atmospheric modelling from
 86 the European Centre for Medium-range Weather Forecasts (ECMWF) and sea surface heights
 87 from the Toulouse Hydrodynamic Unstructured Grid Ocean model (HUGO-m). They analysed
 88 the NTOL signals on 8 SG stations in Central Europe during two storm surge periods of two
 89 weeks, again January-February 2000 and in addition December 2003, with largely improved
 90 correlations of up to 0.8 between gravity and NTOL model predictions. Fenoglio-Marc et al.
 91 (2015) find vertical displacements of 3-5 cm during a storm surge in December 2013 from a
 92 GNSS network of the German North Sea coast and provide maximum correlations of 0.95
 93 between GNSS and ocean models at Heligoland with signal reductions of up to 61 % for a period
 94 of 2 days when correcting the observations with the model values.

95 In this study, we use the high-resolution operational ocean model BSH-HBMnoku
 96 (Brüning et al., 2021) covering the North and Baltic Sea. The NTOL signals from the BSH
 97 model are evaluated on the basis of the gravimetric, Global Navigation Satellite Systems (GNSS)

98 and tide gauge data at Heligoland and compared to the presently available operational products
99 from AOD7 and ECCO2. In addition, NTOL gravity signals from the different models are
100 further evaluated at the continental SG stations Onsala, Serrahn and Strasbourg.
101

102 **2 Data and Methodology**

103 The de-tided and reduced data sets of gravimeters, GNSS sensors and tide gauges at
104 Heligoland are shown in Figure 2 in terms of gravity residuals, vertical displacements and non-
105 tidal sea level variations, respectively, for their available time periods. Details on the data sets,
106 the study site and the methodology can be found in Voigt et al. (2023), while all data reduction
107 steps are described in the following.

108 The continuously operating gravimeters iGrav 047 at Alfred-Wegener-Institute (AWI) at
109 $H_0 = 2.31$ m above mean sea level and the gPhoneX 152 at James-Krüß-Schule (JKS) at $H_0 =$
110 41.35 m are used for cross-validation over a period of 15 months. Due to rather small distances
111 to the coast of 15 m and 230 m, respectively, the observations of both gravimeters at different
112 heights are strongly affected by the direct Newtonian attraction of local water mass variations in
113 the North Sea. The empirical reduction of this local Newtonian attraction from the gravimetric
114 observations is done on the basis of the local tide gauge measurements resulting in height-
115 independent gravity observations ($H_0 = 0$ m). It should be noted that the transfer function
116 between the local sea level and the height-dependent gravity component for iGrav 047 (AWI)
117 from Voigt et al. (2023) has been slightly modified with regard to the analysis of storm surges
118 and sea level heights exceeding the gravimeter height, as suggested there. After reduction of the
119 height-dependent gravity component, the two gravimetric time series are expected to provide
120 identical signals within their uncertainty budgets.

121 These height-independent gravity observations with 1 h time sampling are further
122 reduced by the effects of solid Earth tides and OTL on the basis of local tidal analyses (3 years of
123 iGrav and 16 months of gPhoneX data) with the ET34-X-V80 software (Schueller 2015, 2020),
124 atmospheric mass-redistributions from the Atmospheric Attraction Computation Service
125 (ATMACS; Klügel & Wziontek, 2009) but without the very recently added NTOL term, which
126 accounts for the attraction of the inverted barometer response to the ocean (Antokoletz et al.,
127 2024), and Earth rotation based on the Earth Orientation Parameters (EOPs) provided by the
128 International Earth Rotation and Reference Systems Service (IERS). The vertical displacements
129 in 1 h time sampling from the GNSS stations HELG and HEL2 are processed using the Precise-
130 Point-Positioning (PPP) method and random-walk constrain described in Deng (2023), while the
131 reductions are done according to the IERS conventions 2010. This solution is specifically
132 designed for the analysis of non-tidal ocean loading signals with short duration, and thus
133 contains occasional artificial jumps of up to 10 mm in the coordinate time series at day
134 boundaries. The sea level heights of tide gauge HELBH in the inland harbor next to iGrav 047
135 (AWI) are de-tided by a local tidal analysis based on 22 years of observations with ET34-X-V80
136 while the tide gauge HELSH located at the south harbor of Heligoland has been found to be
137 affected by instrumental issues and natural disturbances (swell, seiches, wind waves), and thus
138 discarded from further study.

139 Both gravity residuals and GNSS vertical displacements in Figures 2a and b are
140 dominated by short-term fluctuations that can be attributed primarily to wind surges according to
141 Figure 2c. On seasonal time scale, the gravity residuals from iGrav 047 (AWI) and the GNSS

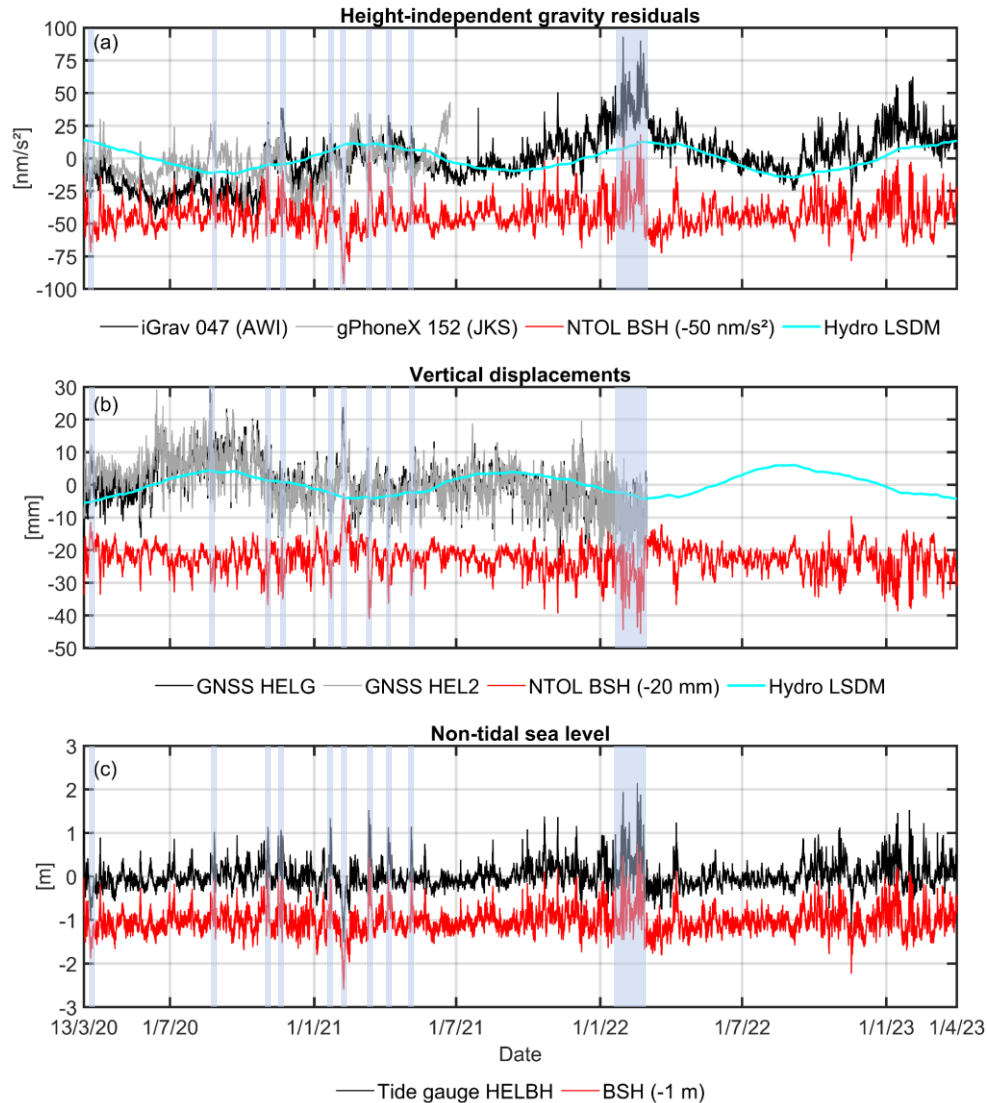


Figure 2. Available data on the island of Heligoland: (a) Height-independent gravity residuals from iGrav 047 (AWI) and gPhoneX 152 (JKS), (b) vertical displacements (positive upwards) from GNSS stations HEL2 and HELG, corresponding values from BSH ocean model and LSDM hydrological model both evaluated at $H_0 = 0$ m, and (c) the non-tidal sea level from local tide gauge HELBH and BSH model. Marked in light blue are the periods under investigation, i.e. nine single weeks in the common gravimeter period with wind surges between 1.0 and 1.5 m deviation from mean high or low water, and an extreme month with several storm surges of more than 1.5 m above mean high water in Jan-Feb 2022. Please note that the BSH model values are shifted vertically to ease readability.

142 vertical displacements show variations attributed to continental water storage variations from the
 143 mainland, while these do not show up significantly in the gPhoneX 152 time series due to the
 144 irregular drift. This is supported by the Land Surface Discharge Model (LSDM; Dill, 2008)
 145 depicted in Figure 2 as well. No significant gravity response could be detected during and after
 146 precipitation events. Hence, most of the precipitation in the vicinity of the gravimeter sites

147 occurs as surface runoff and flows immediately or after a very short delay into the sea. On time
148 scales of a few days, the main target of this study, NTOL signals should be the primary source of
149 gravity variations, especially during storm surges.

150 The shallow-water equation model BSH-HBMnoku covers the North Sea up to a
151 longitude of 4° West and up to a latitude of $60^\circ 15'$ North and the full Baltic Sea (Figure 1). The
152 horizontal resolution is 3 sea miles (5 km), which is densified along the German coasts to 0.5 sea
153 miles (0.9 km). The model is available since 1 Jan 2016 to 5 days in advance with a temporal
154 resolution of 15 min. The computation of the NTOL model predictions is done as follows. We
155 use hourly snapshots of the sea surface height anomalies from the BSH model and 3-hourly
156 snapshots of AOD7 ($1/2^\circ$ resolution) for the domain indicated in Figure 1 and perform first-order
157 conservative remapping with the Climate Data Operator (CDO) software (Schulzweida, 2022) to
158 a resolution of $1/8^\circ$. The obtained load grids and the Gutenberg–Bullen Earth model are used as
159 input for the function NLOADF of the software package SPOTL (Agnew, 2013). The
160 convolution is performed for all timesteps and for each gravimeter station, while the height of
161 station Heligoland is set to zero to obtain the height-independent gravity signatures (Voigt et al.
162 2023). As the BSH model contains both tidal and non-tidal sea level variations, the BSH model
163 predictions are de-tided on the basis of 3 years of data with ET34-X-V80 using the same tidal
164 wave grouping as for the observations.

165 In addition to Heligoland, three additional SG stations are chosen to evaluate the NTOL
166 models according to the two criteria of short distances to the North and Baltic Sea coasts and
167 data availability of gravity residuals for one month with several storm surges from 26 January to
168 25 February 2022. From the database of the International Geodynamics and Earth Tide Service
169 (IGETS; Voigt et al., 2016), the SG stations at Onsala, Serrahn and Strasbourg are selected. The
170 processing and description of gravity residuals (Level 3 data) is described in Boy et al. (2020).

171

172 **3 Results**

173 In order to highlight different features of the gravimetric monitoring on Heligoland, we
174 focus on three different analysis periods. During all comparisons, any offsets between the
175 datasets are reduced for the computation of RMS differences.

176 **3.1 Common observation period at Heligoland**

177 First, we intend to cross-validate the redundant set of gravimeters and GNSS sensors. The
178 comparison of height-independent gravity residuals from iGrav 047 (AWI) and gPhoneX 152
179 (JKS) reveals an RMS difference of 15 nm/s^2 over the full common period of 15 months from 13
180 March 2020 to 23 June 2021. These differences include measurement uncertainties from both
181 gravimeters and the tide gauge for the reduction of the individual height-dependent gravity
182 components, as well as specific local hydrological signals around the gravimeter sites, while
183 atmospheric and large-scale hydrological signals are identical for both instruments and thus
184 cancel out in the differences. The primary source for remaining differences is, however, the
185 highly irregular drift of the gPhoneX, underlining that such spring gravimeters should rather not
186 be used for the monitoring of geophysical signals with periods of some months.

187 The comparison of the vertical displacements from the GNSS stations HEL2 and HELG
188 provides an RMS difference of 3 mm over the full common period. In contrast to the gravimetric

189 data sets, the uncertainties of the vertical displacements from the two GNSS solutions are highly
190 correlated by common systematic effects induced by, e.g., observing the same satellites at the
191 same times. In total, the uncertainty of the 1h vertical displacements from the GNSS solutions
192 appears to be at the level of 1 cm. The correlations between the height-independent gravity
193 residuals and the vertical displacements are up to -0.66 for iGrav 047 (AWI) and -0.30 for
194 gPhoneX 152 (JKS), respectively. This again corroborates deficiencies of the gPhoneX on longer
195 time scales, but also reflects strong common signals in both iGrav and GNSS time series, namely
196 the large-scale NTOL.

197 The comparison of the observational gravity residuals with the predicted signals from the
198 BSH model over the full common period reveals correlations of 0.50 and 0.45 as well as signal
199 reductions of 8 and 6 % when subtracting the NTOL predictions of the BSH model from the
200 gravity residuals of iGrav 047 (AWI) and gPhoneX 152 (JKS), respectively. For GNSS, the
201 results are slightly better with correlations of 0.55 between GNSS vertical displacements and
202 BSH model as well as signal reductions of 15 %. The smaller reduction of the gravity residuals is
203 caused by residual local uncertainties still included in the time series, while GNSS is not
204 sensitive to local effects but only to the elastic deformation of the crust, which effectively acts as
205 a spatial low-pass filter where even highly localized time-variable surface loads (like artificial
206 water reservoirs) cause spatially correlated deformations many kilometers away.

207 3.2 Nine single weeks within the common observation period with strong wind surge 208 events at Heligoland

209 Secondly, we show some examples of exceptionally strong NTOL signals by focusing on
210 nine single weeks with wind surge leading to sea-level anomalies of up to 1.5 m (Figure 2c). The
211 RMS difference of iGrav and gPhone improves drastically by a factor of 5 to 3 nm/s² in average
212 for the 9 periods. This large improvement compared to the full common period clearly shows
213 that the irregular drift of the gPhone is the limiting factor on long time scales. The agreement of
214 the GNSS vertical displacements is 2 mm. The signal-to-noise ratio is better for gravimetry than
215 GNSS for these 1-week intervals suggesting that the wind surge signals over some hours can be
216 resolved more precisely by gravimetry. The correlations between the gravity residuals and GNSS
217 vertical displacements is now -0.70 for all sensor combinations.

218 Correlations between gravity residuals and the BSH model are 0.82 and 0.85 for these
219 nine single weeks, while the signal reduction of the gravity residuals by subtracting the NTOL
220 predictions of the BSH model are 32 and 39 % for iGrav and gPhone, respectively. These figures
221 show that the gPhone can be used adequately for such time intervals. GNSS vertical
222 displacements are correlated with BSH model values by 0.73 (HEL2) and 0.75 (HELG) and
223 signals can be reduced by 33 % on both GNSS stations. In total, these comparisons during single
224 weeks with intense winds further support the conclusion that the observed gravity signals are
225 primarily driven by NTOL.

226 3.3 One month with several storm surges in the German Bight

227 In a third step, we extend the analysis to one month with several storm surges in the
228 German Bight from 26 January to 25 February 2022, and do not only focus on Heligoland but
229 also on three additional SG stations on the continent. Between 30 January and 7 February 2022,
230 six storm surges with at least +1.5 m hit the North Sea coast of Germany. Shortly afterwards
231 from 17 to 22 February 2022, seven additional storm surges induced strong sea-level variations

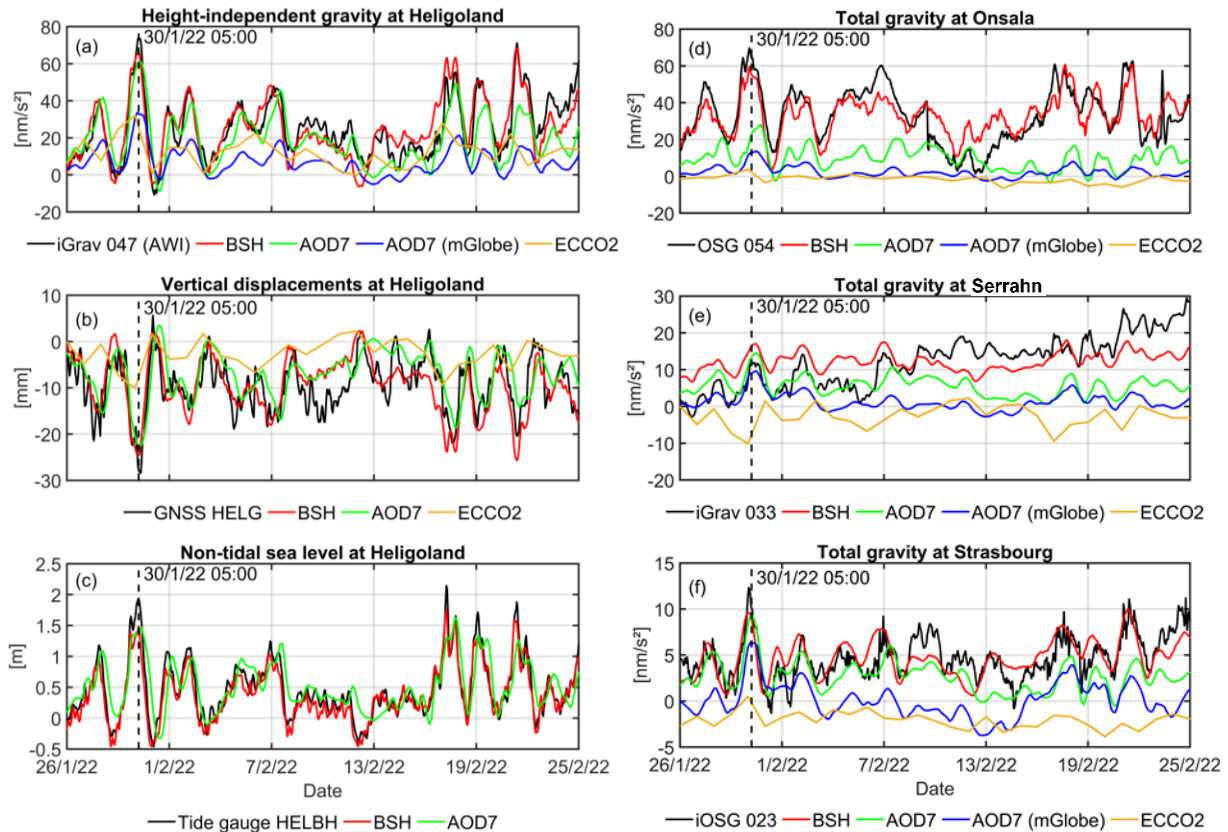


Figure 3. Gravity, GNSS and tide gauge observations at Heligoland with corresponding NTOL model values during one month with several storm surges (a-c), gravity residuals from SG stations at Onsala, Serrahn and Strasbourg with corresponding NTOL model values (d-f). The observations are fitted to the mean values of the corresponding values from the BSH model.

232 (Figure 3c). At 30 January 2022 at 05:00 UTC, maximum storm surge signals reach gravity
 233 increases (peak-to- peak) of up to 85 nm/s² and vertical displacements of -34 mm from
 234 superconducting gravimeter iGrav 047 (AWI) and GNSS HELG observations at Heligoland,
 235 respectively, during increased local sea level heights of +2.0 m above mean high water at
 236 Heligoland. These figures are even larger than the maximum values reported previously by
 237 Fratepietro et al. (2006).

238 The correlations at Heligoland are 0.87 and 0.74 for gravimetry and GNSS, respectively,
 239 with the BSH model. The signal reductions are 50 % for gravity residuals, while GNSS shows
 240 only half of this amount which is still very significant. Hence, during extreme conditions
 241 gravimetry can resolve much better the NTOL signals than GNSS (Figures 3a and b). We also
 242 exchange model predictions from BSH with other NTOL datasets frequently used in the gravity
 243 community. Ocean bottom pressure anomalies from MPIOM that are also used for the GRACE
 244 Non-tidal dealiasing model AOD1B RL07 (Shihora et al., 2022) have been used with SPOTL to
 245 calculate NTOL effects (denoted as AOD7). Please note that these time series are currently
 246 prepared for incorporation into ATMACS (Antokoletz et al., 2024). We also utilize the publicly
 247 available Stokes coefficients of AOD1B RL07 and process NTOL with the mGlobe package
 248 (Mikolaj et al., 2016) and predictions based on ECCO2 available from the EOST loading service

249 (Table 1). We note that the amplitudes from AOD7 (processed with SPOTL) are much larger
250 than the corresponding amplitudes from AOD7 (mGlobe), suggesting that there is a significant
251 signal attenuation resulting from coastline resolution limitations in mGlobe that are particularly
252 relevant for coastal stations as Heligoland. We also note an apparent time lag of 3-4 hours for
253 both AOD7 solutions in comparison with the observations indicating systematic delays in the
254 storm surges in the German Bight in the underlying MPIOM simulation, which will require
255 further investigations.

256 The NTOL signals from all four models are computed also for the IGETS SG stations
257 Onsala, Serrahn and Strasbourg. In total, the agreements are weaker than at Heligoland as the
258 NTOL signals are not the primary contributor to the gravity residuals but terrestrial water storage
259 changes coming into play in addition to instrumental disturbances in the gravity residuals
260 automatically processed by IGETS. Again, the BSH model consistently shows by far the best
261 agreements with the gravimetric observations. But there are significant improvements in
262 correlation and signal reductions on all stations from 10 % (Serrahn) to 39 % signal reduction
263 (Onsala). This is different for the two AOD7 solutions. Although the major NTOL peaks are
264 visible in both solutions, AOD7 reveals weaknesses for stations near the semi-enclosed Baltic
265 Sea (Onsala, Serrahn), while it performs well at Strasbourg which is more affected by the North
266 Sea. However, AOD7 (mGlobe) and ECCO2 provide signal reductions of up to 8 % only on any
267 of the stations considered. We also note that the results at Strasbourg might be improved even
268 further by combining the results from the regional BSH model with a global model like AOD7 to
269 cover also signals from the Biskaya.

270 Figure 3 also reveals that vertical displacements from GNSS suffer from systematic
271 effects and enhanced noise at subdaily time scales which greatly limits resolving the storm surge
272 signals. Gravity residuals from iGrav 047 together with a mean height-to-gravity ratio for NTOL
273 derived from the BSH model might be thus used as a proxy to estimate gravimetry-based vertical
274 displacements that are fully independent of GNSS. The mean gravity-to-height ratio (dg/dh)
275 from the BSH model during the investigated month with several storm surges is -2.684 (0.003)
276 nm/s^2 per mm vertical displacement, which is very stable and close to the results from
277 Fratepietro et al. (2006). A NTOL gravity signal of 80 nm/s^2 observed with an RMSE of 2 nm/s^2
278 could thus be transformed into a vertical displacement of 29.8 mm with an RMSE of 0.7 mm
279 only. This solution improves the agreement between gravimetry-based vertical displacements
280 and BSH as well as AOD7 to end up with the same results as for gravimetry in terms of
281 correlation and signal reduction, which appears to be a promising path for a possible
282 incorporation of superconducting gravimeters for vertical reference frame realizations as long as
283 local hydrological signals are small in (or sufficiently well reduced from) the gravimetric
284 observations.

Table 1. Descriptive statistics of the comparison between observations and NTOL model values in terms of correlation and reduction of gravity residuals (RMS) during one month (26 Jan to 25 Feb 2022) with several storm surges according to Figure 3.

Station	Functional	Correlation / Reduction			
		BSH	AOD7	AOD7 (mGlobe)	ECCO2
Heligoland	Height-independent gravity	0.87 / 49 %	0.77 / 36 %	0.69 / 24 %	0.35 / 6 %
Onsala	Total gravity	0.80 / 39 %	0.17 / -1 %	0.50 / 8 %	0.12 / 8 %
Serrahn	Total gravity	0.44 / 10 %	-0.07 / -9 %	-0.05 / -6 %	0.18 / 0 %
Strasbourg	Total gravity	0.63 / 19 %	0.53 / 13 %	0.40 / -1 %	0.19 / 1 %
Heligoland	Vertical displacements	0.74 / 25 %	0.69 / 24 %	- / -	0.33 / 5 %

285

286 **4 Conclusions**

287 With a unique set of partially redundant geodetic instruments consisting of gravimeters,
 288 GNSS stations, and tide gauges on the small island of Heligoland in the North Sea, we
 289 demonstrate that the dedicated regional ocean model BSH-HBMnoku explains large fractions of
 290 the observed regional NTOL signals. For a particularly stormy month in winter 2022,
 291 correlations of 0.9 and signal reductions of 50 % are found when reducing NTOL model
 292 predictions from gravimetric observations. This is a significant improvement against more
 293 commonly used global NTOL products provided by the EOST loading service or the mGlobe
 294 package. For stations in Central Europe, a combination of the regional model BSH-HBMnoku
 295 with a global model to include also NTOL signals from the Biskaya and the Mediterranean Sea
 296 might improve the results even further. Our analysis also provides insights into further possible
 297 improvements of global NTOL models, most notably with respect to an apparent time-lag of 3
 298 to 4 hours in AOD7 with respect to the geodetic observations. The continued operation of iGrav
 299 047 on Heligoland will continue to provide ground truth information for future NTOL model
 300 development.

301 We also find that gPhoneX spring gravimeters are very well suited for the analysis of
 302 NTOL signals over periods of roughly one week in almost the same way as SGs, but not for
 303 longer periods due to their highly irregular drift behaviours. In view of the much lower
 304 complexity of a spring gravimeter compared to an iGrav, this opens an interesting opportunity to
 305 observe the evolution of storm surges in real-time with instruments that can be operated well
 306 sheltered away from the weather. We intend to continue this research by operating gPhoneX
 307 instruments at a number of places in close proximity to the coasts but otherwise very differing
 308 environmental conditions to further study the versatility of this instrument for oceanographic
 309 applications.

310

311 **Acknowledgments**

312 This project is funded by the Deutsche Forschungsgemeinschaft (DFG, German Research
 313 Foundation) – Project-ID 434617780 – SFB 1464, and under Germany’s Excellence Strategy –
 314 EXC – 2123 QuantumFrontiers – 390837967 at Leibniz Universität Hannover. Additional
 315 support was available from the TIDUS project within the research unit NEROGRAV (DFG

316 Research Unit 2736, Grants: TH864/15-1, DE2174/12-1). The Helgoland Gravimetric
317 Observatory Germany (HELGOG) is part of the Modular Earth Science Infrastructure (MESI) of
318 the GFZ. We thank the Biologische Anstalt Helgoland of AWI for providing a suitable location
319 for this observatory and for technical support. We thank the Institute of Geosciences, Christian-
320 Albrechts-Universität zu Kiel for hosting the gPhoneX at the seismological station Helgoland at
321 JKS. At the Federal Maritime and Hydrographic Agency (BSH), we thank Andreas Boesch from
322 the tidal information service for valuable input and the team from operational modelling for
323 assistance with BSH-HBM data. The Generic Mapping Tools (GMT; Wessel and Smith, 1998)
324 were used to prepare Figure 1.
325

326 **Data Availability**

327 All datasets used within this study are publicly available. Gravity and barometric pressure data
328 from the gravimeters iGrav 047 and gPhoneX 152 at Heligoland (Voigt et al., 2020) as well as
329 from OSG 054 at Onsala (Scherneck et al., 2022), iGrav 033 at Serrahn (Reich et al., 2024) and
330 iOSG 023 at Strasbourg (Boy et al., 2017) are available from the IGETS database hosted by the
331 Information System and Data Center at GFZ (Voigt et al., 2016). Raw GNSS data are available
332 from BKG (2024), while processed data are published by Deng (2023). The sea level heights
333 from the tide gauges HELBH and HELSH are available for the past 30 days from WSV (2024),
334 while long time-series are available upon request from BfG (2024). The operational ocean model
335 BSH-HBMnoku is available from BSH (2024).
336

337 **References**

- 338 Agnew, D.C., 2013. SPOTL: some programs for ocean-tide loading, Scripps Institution of
339 Oceanography Technical Report, University of California, Available at:
340 <https://igppweb.ucsd.edu/~agnew/Spotl/spotlmain.html> (last access: 6 Mar 2024).
- 341 Antokoletz, E. D., Wziontek, H., Dobsław, H., Balidakis, K., Klügel, T., Oreiro, A. & Tocho, C.
342 N., 2024. Combining atmospheric and non-tidal ocean loading effects to correct high precision
343 gravity time-series, *Geophys. J. Int.*, 236, 88-98, DOI: 10.1093/gji/ggad371.
- 344 BfG, 2024. Datenstelle der Bundesanstalt für Gewässerkunde. Email: Datenstelle-M1@bafg.de.
- 345 BKG, 2024. The BKG GNSS Data Center, Available at: <https://igs.bkg.bund.de/> (last access: 7
346 Mar 2024).
- 347 Boy, J.-P. & Lyard, F., 2008. High-frequency non-tidal ocean loading effects on surface gravity
348 measurements, *Geophys. J. Int.*, 175, 35-45, DOI: 10.1111/j.1365-246X.2008.03895.x
- 349 Boy, J.-P., Rosat, S., Hinderer, J. & Littel, F., 2017. Superconducting Gravimeter Data from
350 Strasbourg - Level 1, GFZ Data Services, DOI: 10.5880/igets.st.11.001.
- 351 Boy, J.-P., Barriot, J.-P., Förste, C., Voigt, C. & Wziontek, H., 2020. Achievements of the first 4
352 years of the International Geodynamics and Earth Tide Service (IGETS) 2015–2019, in *Beyond*

- 353 *100: The Next Century in Geodesy. International Association of Geodesy Symposia*, 152, eds
354 Freymueller, J.T. & Sánchez, L., Springer, DOI: 10.1007/1345_2020_94.
- 355 Boy, J.-P., 2024. EOST Loading Service, URL: <http://loading.u-strasbg.fr> (last access: 6 Feb
356 2024).
- 357 Brüning, T., Li, X., Schwichtenberg, F. & Lorkowski, I., 2021. An operational, assimilative
358 model system for hydrodynamic and biogeochemical applications for German coastal waters,
359 *Hydrographische Nachrichten/Journal of Applied Hydrography*, 118, 6-15, DOI:
360 10.23784/HN118-01.
- 361 BSH, 2024. Operational Modelling of the Federal Maritime and Hydrographic Agency (BSH),
362 URL: <https://data.bsh.de/OpenData/OperationalModel/> (last access: 13 Feb 2024).
- 363 Deng, Z., 2023. Heligoland GNSS hourly time series positioning for 2017-2021, GFZ Data
364 Services, DOI: 10.5880/GFZ.1.1.2023.001.
- 365 Dill, R., 2008. Hydrological model LSDM for operational Earth rotation and gravity field
366 variations. GFZ Scientific Technical Report STR08/09, DOI: 11.2312/GFZ.b103-08095.
- 367 Dobslaw, H., Bergmann-Wolf, I., Dill, R., Poropat, L., Thomas, M., Dahle, C., Esselborn, S.,
368 König, R. & Flechtner, F., 2017. A new high-resolution model of non-tidal atmosphere and
369 ocean mass variability for de-aliasing of satellite gravity observations: AOD1B RL06, *Geophys.*
370 *J. Int.*, 211, 1, 263-269, DOI: 10.1093/gji/ggx302.
- 371 Fenoglio-Marc, L., Scharroo, R., Annunziato, A., Mendoza, L., Becker, M. & Lillibridge, J.,
372 2015. Cyclone Xaver seen by geodetic observations, *Geophys. Res. Lett.*, 42, 9925-9932, DOI:
373 10.1002/2015GL065989.
- 374 Fratepietro, F., Baker, T. F., Williams, S. D. P. & Van Camp, M., 2006. Ocean loading
375 deformations caused by storm surges on the northwest European shelf, *Geophys. Res. Lett.*,
376 33(6), DOI: 10.1029/2005GL025475.
- 377 Klügel, T. & Wziontek, H., 2009. Correcting gravimeters and tiltmeters for atmospheric mass
378 attraction using operational weather models, *J. Geodyn.*, 48, 204–210, DOI:
379 10.1016/j.jog.2009.09.010.
- 380 Mikolaj, M., Meurers, B. & Güntner, A., 2016. Modelling of global mass effects in hydrology,
381 atmosphere and oceans on surface gravity, *Comput. Geosci.*, 93, 12–20, DOI:
382 10.1016/j.cageo.2016.04.014.
- 383 Reich, M., Güntner, A. & Schröder, S., 2024. Superconducting Gravimeter Data from Serrahn -
384 Level 1, GFZ Data Services, DOI: 10.5880/igets.se.11.001.
- 385 Scherneck, H.-G., Mouyen, M. & Reldin, J., 2022. Superconducting Gravimeter Data from
386 Onsala - Level 1, GFZ Data Services, DOI: 10.5880/igets.os.11.001.

- 387 Schueller, K., 2015. Theoretical Basis for Earth Tide Analysis with the New ETERNA34-ANA-
388 V4.0 Program, *Bulletin d'Information des Marées Terr.*, 149, 12024–12061, [http://maregraph-
renater.upf.pf/bim/BIM/bim149.pdf](http://maregraph-
389 renater.upf.pf/bim/BIM/bim149.pdf)
- 390 Schueller, K., 2020. Program System ETERNA-x et34-x-v80 for Earth and Ocean Tides
391 Analysis and Prediction, Documentation Manual 01: Theory and 02: Users Guide. Technical
392 reports, Institution: <http://ggp.bkg.bund.de/eterna?download=7283>
- 393 Schulzweida, U., 2022. CDO User Guide (2.1.0), Zenodo, DOI: 10.5281/zenodo.7112925.
- 394 Shihora, L., Balidakis, K., Dill, R. & Dobslaw, H., 2022. Atmosphere and Ocean Non-Tidal
395 Dealiasing Level-1B (AOD1B) Product RL07, GFZ Data Services. DOI:
396 10.5880/GFZ.1.3.2022.003
- 397 Voigt, C., Förste, C., Wziontek, H., Crossley, D., Meurers, B., Palinkas, V., Hinderer, J., Boy, J.-
398 P., Barriot, J.-P. & Sun, H., 2016. Report on the data base of the international geodynamics and
399 earth tide service (IGETS), Scientific technical report STR Potsdam, GFZ German Research
400 Centre for Geosciences, Potsdam, Germany, DOI: 10.2312/gfz.b103-16087.
- 401 Voigt, C., Stolarczuk, N., Pflug, H., Förste, C., Flechtner, F., Peters, H. & Fietz, M., 2020.
402 Superconducting Gravimeter Data from Helgoland - Level 1, GFZ Data Services, DOI:
403 10.5880/igets.he.11.001.
- 404 Voigt, C., Sulzbach, R., Timmen, L., Dobslaw, H., Weise, A., Deng, Z., Stolarczuk, N., Pflug,
405 H., Peters, H., Fietz, M., Thomas, M., Förste, C. & Flechtner, F., 2023. A superconducting
406 gravimeter on the island of Heligoland for the high-accuracy determination of regional ocean
407 tide loading signals of the North Sea, *Geophys. J. Int.*, 234(3), 1585–1602. DOI:
408 10.1093/gji/ggad147
- 409 Weise, A., Timmen, L., Deng, Z., Gabriel, G., Rothleitner, C., Schilling, M. & Voigt, C., 2020.
410 Observing Ocean Mass Variability with Spring Gravimeters – Storm Surge Induced Signals on
411 the North Sea Island Helgoland, *AVN Allgemeine Vermessungsnachrichten*, 127, 4, 163-173.
- 412 Wessel, P. & Smith, F., 1998. New, improved version of generic mapping tools released, EOS,
413 79, 579. DOI: 10.1029/98EO00426.
- 414 WSV, 2024. Pegelonline. URL:
415 <https://www.pegelonline.wsv.de/webservices/files/Wasserstand+Rohdaten/NORDSEE> (last
416 access: 13 Feb 2024).